Design of Doubly-Connected Metalenses for Conformal Array Transformation

M. Salucci, A. Polo, and G. Oliveri

Abstract

In this work, a novel transformation electromagnetics technique based on the Schwarz-Christoffel (SC) theory is proposed to synthesize effective field manipulation devices. Thanks to such a methodology it is possible to design meta-material coatings for conformal linear phased arrays having a doubly-connected profile with reduced anisotropy. Preliminary numerical results are shown in order to validate the developed transformation tool on a selected benchmark scenario.

Contents

1 Mathematical Formulation

1.1 Schwarz-Christoffel Transformation

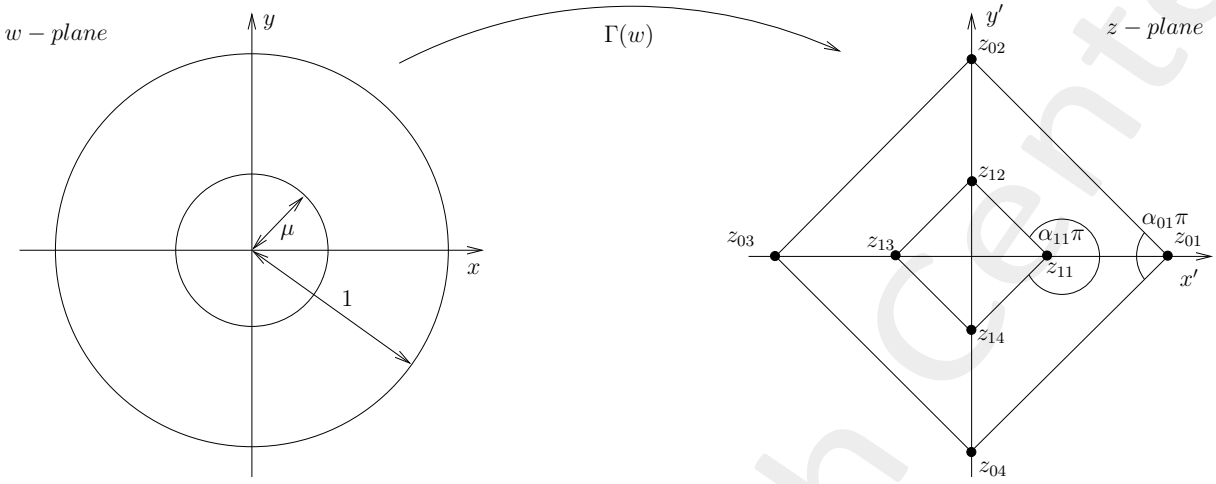

Figure 1: Mapping through Schwarz-Christoffel Transformation

Given Figure (1), the virtual points of a double-connected region R_μ $(w - plane)$ will be mapped into a new physical geometry L $(z - plane)$ by means of the Schwarz-Christoffel transformation

$$\Gamma(w) = \Gamma(w_c) + C \int_{w_c}^{w} \prod_{k=1}^{M} \left[\Theta\left(\frac{\zeta}{\mu w_{0k}}\right)\right]^{\alpha_{0k}-1} \prod_{k=1}^{N} \left[\Theta\left(\frac{\mu\zeta}{w_{1k}}\right)\right]^{\alpha_{1k}-1} d\zeta \tag{1}$$

where

- $C \in \mathbb{C}$ is a complex constant
- $M,\ N$ are the number of discretization points of the respectively outer and inner polygon of the physical geometry L
- μ is the inner radius of R_μ
- $\{z_{0k}\}_{k=1}^{M},\ \{z_{1k}\}_{k=1}^{N}$ are the vertices of the respectively outer and inner polygon (numbered counterclockwise)
- $\{w_{0k}\}_{k=1}^{M},\ \{w_{1k}\}_{k=1}^{N}$ are the prevertices of the respectively outer and inner vertices of L defined as:

$$\begin{cases} \{w_{0k}\}_{k=1}^{M} = \Gamma'\left(\{z_{0k}\}_{k=1}^{M}\right) \\ \{w_{1k}\}_{k=1}^{N} = \Gamma'\left(\{z_{1k}\}_{k=1}^{N}\right) \end{cases} \tag{2}$$

  where Γ' is the inverse transformation from $z - plane$ to $w - plane$

- w_c is the nearest prevertix of w

- $\{\alpha_{0k}\pi\}_{k=1}^{M},\ \{\alpha_{1k}\pi\}_{k=1}^{N}$ are the internal angles satisfying:

$$\begin{cases} \sum_{k=1}^{M} \alpha_{0k} = M - 2 \\ \sum_{k=1}^{N} \alpha_{1k} = N + 2 \end{cases} \tag{3}$$

Finally $\Theta(w, \mu)$ is defined as

$$\Theta(w, \mu) = \prod_{j=1}^{\infty} \left(1 - \mu^{2j-1} w\right) \left(1 - \mu^{2j-1} w^{-1}\right). \tag{4}$$

Considering an arbitrary inner radius μ' for R_μ, a scaling factor τ will be computed as:

$$\tau = \frac{\mu'}{\mu} \tag{5}$$

and the outer radius of the virtual geometry will be assigned to τ.

1.1.1 Compensation Angle

Given a control point in the virtual region $\underline{w} = (\rho_{cp}, \varphi_{cp})$ we would like that the same point in the physical region keeps the same angle φ_{cp}, i.e.,

$$\underline{w} = (\rho_{cp}, \varphi_{cp}) \rightarrow \underline{z} = \Gamma(\underline{w}) = (\rho'_{cp}, \varphi_{cp}) \tag{6}$$

Towards this goal, a compensation angle is computed as follows:

1. Considering the control point $\underline{z} = (\rho'_{cp}, \varphi'_{cp})$ in the physical region forcing that $\varphi'_{cp} = \varphi_{cp}$, the equivalent point in the virtual region is computed as

$$\underline{w} = \Gamma'(\underline{z}) = (\rho'', \varphi'') \tag{7}$$

   where we want that $\varphi'' = \varphi_{cp}$. The radius ρ'_{cp} is selected considering the further point on the internal polygon from the origin as

$$\rho'_{cp} = \max_{\rho'} \left\{ \{z_{1k}\}_{k=1}^{N} \right\} + \Upsilon \tag{8}$$

   being Υ an offset.

2. The compensation angle is computed as

$$\Theta = \varphi_{cp} - \varphi'' \tag{9}$$

The points in the virtual region will be mapped into the physical one after applied the compensation angle as

$$\underline{w} = (\rho, \varphi - \Theta) = (\rho, \varphi - \varphi_{cp} + \varphi'') \tag{10}$$

So considering $\underline{w} = (\rho_{cp}, \varphi_{cp})$

$$\underline{w} = (\rho_{cp}, \varphi_{cp} - \Theta) = (\rho_{cp}, \varphi_{cp} - \varphi_{cp} + \varphi'') = (\rho_{cp}, \varphi'') \tag{11}$$

and the point will be transformed as

$$\underline{z} = \Gamma(\underline{w}) = (\rho'_{cp}, \varphi'_{cp}) \tag{12}$$

where at beginning we enforce that $\varphi'_{cp} = \varphi_{cp}$.

1.2 Lens Definition

Treating doubly-connected regions, the cylindrical coordinates are preferred. Starting from the virtual region described by a (ρ, φ, z) coordinates, using Schwarz-Christoffel transformation as just explained, we will define a new physical geometry defined by the new coordinates (ρ', φ', z'):

$$(\rho', \varphi', z') = \Gamma(\rho, \varphi, z) \tag{13}$$

The physical geometry will be a doubly-connected structure representing the lens containing the array. The lens is described by the $\underline{\underline{\varepsilon}}'(x', y')$, $\underline{\underline{\mu}}'(x', y')$ tensors of permittivity and permeability, respectively. In order to compute the $\underline{\underline{\varepsilon}}'$, $\underline{\underline{\mu}}'$ tensors in a (x', y') point, it is needed to compute the Jacobian matrix of the transformation defined by:

$$[\Lambda] = \begin{bmatrix} \frac{\partial \rho'}{\partial \rho} & \frac{\partial \rho'}{\partial \varphi} & \frac{\partial \rho'}{\partial z} \\ \frac{\partial \varphi'}{\partial \rho} & \frac{\partial \varphi'}{\partial \varphi} & \frac{\partial \varphi'}{\partial z} \\ \frac{\partial z'}{\partial \rho} & \frac{\partial z'}{\partial \varphi} & \frac{\partial z'}{\partial z} \end{bmatrix} = \begin{bmatrix} \frac{\partial \rho'}{\partial \rho} & \frac{\partial \rho'}{\partial \varphi} & 0 \\ \frac{\partial \varphi'}{\partial \rho} & \frac{\partial \varphi'}{\partial \varphi} & 0 \\ 0 & 0 & 1 \end{bmatrix} \tag{14}$$

where after some manipulations, the final matrix $[\Lambda_T]$ it will be

$$[\Lambda_T] = \begin{bmatrix} 1 & 0 & 0 \\ 0 & \rho' & 0 \\ 0 & 0 & 1 \end{bmatrix} [\Lambda] \begin{bmatrix} 1 & 0 & 0 \\ 0 & \frac{1}{\rho} & 0 \\ 0 & 0 & 1 \end{bmatrix} \tag{15}$$

$$[\Lambda_T] = \begin{bmatrix} \frac{\partial \rho'}{\partial \rho} & \frac{1}{\rho}\frac{\partial \rho'}{\partial \varphi} & 0 \\ \rho' \frac{\partial \varphi'}{\partial \rho} & \frac{\rho'}{\rho}\frac{\partial \varphi'}{\partial \varphi} & 0 \\ 0 & 0 & 1 \end{bmatrix} \tag{16}$$

Finally, in order to implement the computation of the matrix in a software, we consider the partial derivatives as follows (Fig.2).

$$[\Lambda'] = \begin{bmatrix} \frac{d\rho'_\rho}{d\rho} & \frac{1}{\rho}\frac{d\rho'_\varphi}{d\varphi} & 0 \\ \rho' \frac{d\varphi'_\rho}{d\rho} & \frac{\rho'}{\rho}\frac{d\varphi'_\varphi}{d\varphi} & 0 \\ 0 & 0 & 1 \end{bmatrix} \tag{17}$$

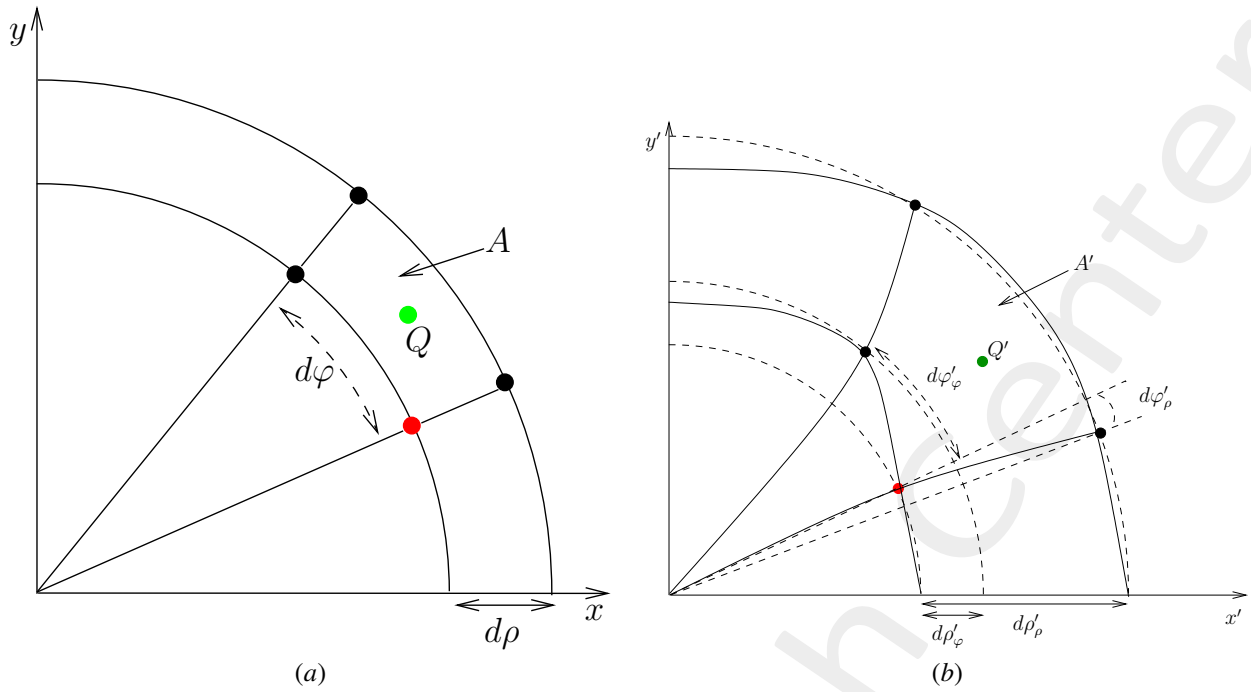

Figure 2: Elementary cell and partial derivatives in the (*a*) virtual and (*b*) physical geometries

Computed the Jacobian matrix, it is possible to compute the entries of $\underline{\underline{\varepsilon}}'$, $\underline{\underline{\mu}}'$ tensors in a point of the physical domain (x', y') as follows

$$\underline{\underline{\varepsilon}}'(x', y') = \begin{bmatrix} \varepsilon'_{\rho\rho} & \varepsilon'_{\rho\theta} & \varepsilon'_{\rho z} \\ \varepsilon'_{\theta\rho} & \varepsilon'_{\theta\theta} & \varepsilon'_{\theta z} \\ \varepsilon'_{z\rho} & \varepsilon'_{z\theta} & \varepsilon'_{zz} \end{bmatrix} = \frac{\underline{\underline{\Lambda}}_T \, \underline{\underline{\varepsilon}} \, \underline{\underline{\Lambda}}_T^T}{det(\underline{\underline{\Lambda}}_T)} \tag{18}$$

$$\underline{\underline{\mu}}'(x', y') = \begin{bmatrix} \mu'_{\rho\rho} & \mu'_{\rho\theta} & \mu'_{\rho z} \\ \mu'_{\theta\rho} & \mu'_{\theta\theta} & \mu'_{\theta z} \\ \mu'_{z\rho} & \mu'_{z\theta} & \mu'_{zz} \end{bmatrix} = \frac{\underline{\underline{\Lambda}}_T \, \underline{\underline{\mu}} \, \underline{\underline{\Lambda}}_T^T}{det(\underline{\underline{\Lambda}}_T)} \tag{19}$$

where $\underline{\underline{\varepsilon}}$, $\underline{\underline{\mu}}$ are the permittivity/permeability tensors in the virtual space (Figure 3) while $\underline{\underline{\Lambda}}_T^T$ is the transpose matrix of the Jacobian.

1.3 Tensors Conversion

In the simulation of the physical geometry, we need to consider the Cartesian tensors of permittivity and permeability. In order to convert the tensors, we will consider the following transformation matrix

$$[W] = \begin{bmatrix} cos(\varphi) & sin(\varphi) & 0 \\ -sin(\varphi) & cos(\varphi) & 0 \\ 0 & 0 & 1 \end{bmatrix} \tag{20}$$

where φ is the counterclockwise angle from the $x - axis$ in the $x - y$ plane computed as:

$$\varphi = \begin{cases} 2arctan\left(\frac{y}{\sqrt{x^2+y^2}+x}\right) & \text{if } x > 0 \text{ or } y \neq 0 \\ \pi & \text{if } x < 0 \text{ and } y = 0 \\ \text{undefined} & \text{if } x = 0 \text{ and } y = 0 \end{cases} \tag{21}$$

Therefore in the physical geometry the φ angle is computed considering the coordinates (x', y') of Q' the centroid of the elementary cell in which is computed the permittivity and permeability tensor. So the Cartesian tensor of permittivity/permeability will be transformed as

$$\underline{\underline{\varepsilon}}(x', y') = \begin{bmatrix} \varepsilon'_{xx} & \varepsilon'_{xy} & \varepsilon'_{xz} \\ \varepsilon'_{yx} & \varepsilon'_{yy} & \varepsilon'_{yz} \\ \varepsilon'_{zx} & \varepsilon'_{zy} & \varepsilon'_{zz} \end{bmatrix} = [W^T] \begin{bmatrix} \varepsilon'_{\rho\rho} & \varepsilon'_{\rho\theta} & \varepsilon'_{\rho z} \\ \varepsilon'_{\theta\rho} & \varepsilon'_{\theta\theta} & \varepsilon'_{\theta z} \\ \varepsilon'_{z\rho} & \varepsilon'_{z\theta} & \varepsilon'_{zz} \end{bmatrix} [W] \tag{22}$$

$$\underline{\underline{\mu}}(x', y') = \begin{bmatrix} \mu'_{xx} & \mu'_{xy} & \mu'_{xz} \\ \mu'_{yx} & \mu'_{yy} & \mu'_{yz} \\ \mu'_{zx} & \mu'_{zy} & \mu'_{zz} \end{bmatrix} = [W^T] \begin{bmatrix} \mu'_{\rho\rho} & \mu'_{\rho\theta} & \mu'_{\rho z} \\ \mu'_{\theta\rho} & \mu'_{\theta\theta} & \mu'_{\theta z} \\ \mu'_{z\rho} & \mu'_{z\theta} & \mu'_{zz} \end{bmatrix} [W] \tag{23}$$

where $\underline{\underline{W^T}}$ is the transpose matrix.

The lens can be approximated to an isotropic one considering the following tensors

$$\underline{\underline{\varepsilon}}' = \begin{bmatrix} \varepsilon'_r & 0 & 0 \\ 0 & \varepsilon'_r & 0 \\ 0 & 0 & \varepsilon'_r \end{bmatrix} \tag{24}$$

$$\underline{\underline{\mu}}' = \begin{bmatrix} 1 & 0 & 0 \\ 0 & 1 & 0 \\ 0 & 0 & 1 \end{bmatrix} \tag{25}$$

for a TM propagation mode, where $\varepsilon'_r(x', y')$ is a constant computed as

$$\varepsilon'_r = \frac{A}{A'} \tag{26}$$

A being the area of the discretization cell with centroid in $Q = (x, y)$ for the virtual case while A' is the area of the discretization cell in the physical domain with centroid defined in $Q' = (x', y')$.

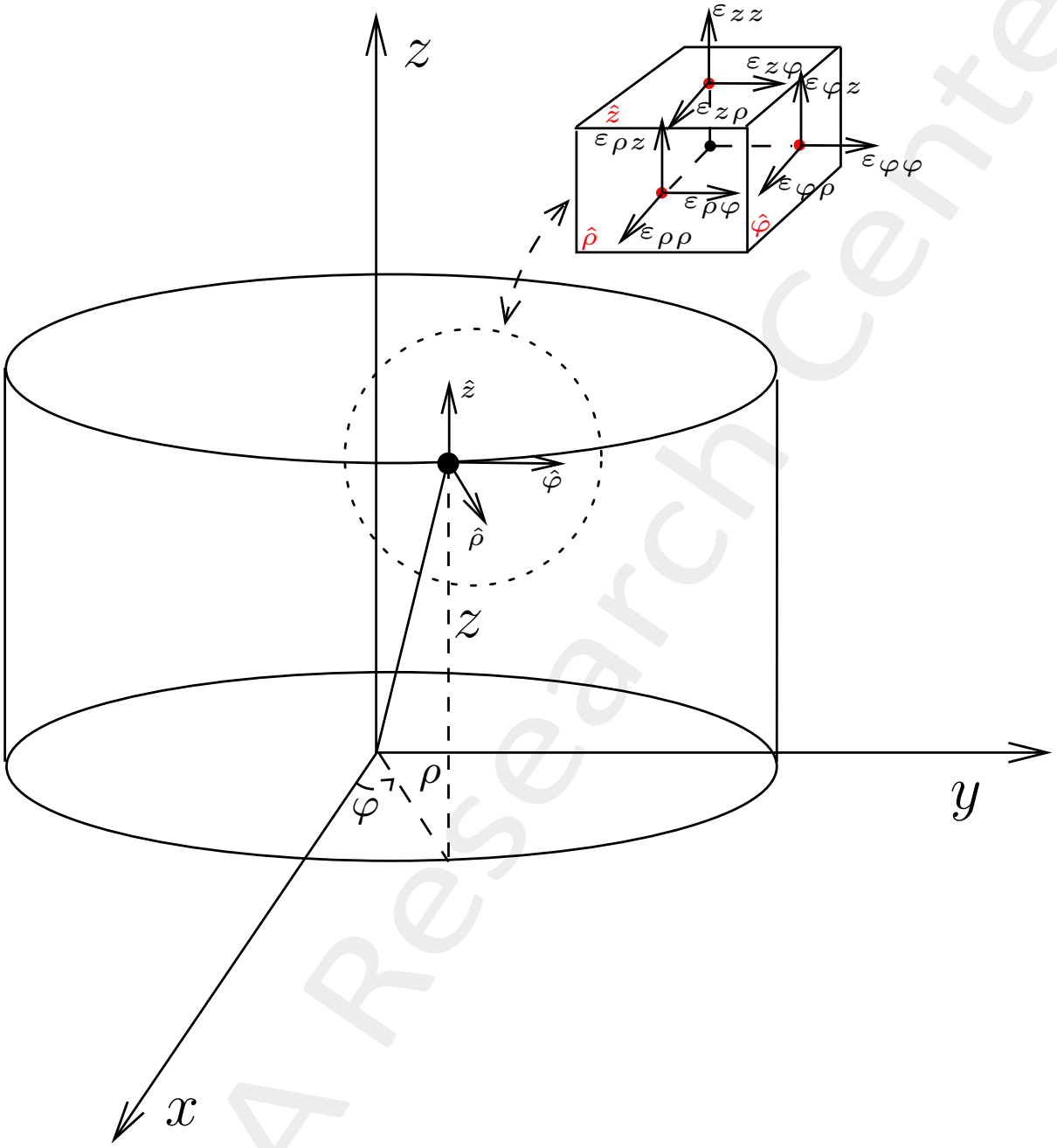

Figure 3: Permittivity tensor expressed in the cylindrical coordinates

1.4 Definitions

- Maximum directivity

$$D_{max}(\theta,\varphi) = \frac{4\pi \max_{(\theta,\varphi)}\{|E(\theta,\varphi)|^2\}}{\int_0^{2\pi}\int_0^{\pi}|E(\theta,\varphi)|^2\sin(\theta)d\theta d\varphi} \tag{27}$$

- Sidelobe level (SLL)

$$SLL = 20 \times log_{10}\left(\frac{\max\{F(\theta,\varphi)\}}{\max\{E(\theta,\varphi)\}}\right) \tag{28}$$

where $F(\theta,\varphi)$ is the $E(\theta,\varphi)$ secondary lobes

- Maximum lens permittivity

$$\max\{\underline{\underline{\varepsilon}}\} = \max_{\underline{r}\in\Omega}\{\varepsilon_{pq}(\underline{r});\ p,q\ \in\{1,2,3\}\} \tag{29}$$

- Minimum lens permittivity

$$\min\{\underline{\underline{\varepsilon}}\} = \min_{\underline{r}\in\Omega}\{\varepsilon_{pq}(\underline{r});\ p,q\ \in\{1,2,3\}\} \tag{30}$$

- Average fractional anisotropy

$$\alpha_F = \frac{1}{area(\Omega)}\int_{\underline{r}\in\Omega}\sqrt{\frac{3\sum_{i=1}^{3}[\sigma_i(\underline{r})-\sigma_{ave}(\underline{r})]^2}{2\sum_{i=1}^{3}[\sigma_i(\underline{r})]^2}}d\underline{r} \tag{31}$$

- Average relative anisotropy

$$\alpha_R = \frac{1}{area(\Omega)}\int_{\underline{r}\in\Omega}\sqrt{\frac{\sum_{i=1}^{3}[\sigma_i(\underline{r})-\sigma_{ave}(\underline{r})]^2}{3\sigma_{ave}(\underline{r})}}d\underline{r} \tag{32}$$

where

  - $\sigma_i(\underline{r}),\ i=1,...,3$ are the eigenvalues of the permittivity tensor $\underline{\underline{\varepsilon}}(\underline{r})$;
  - $\sigma_{ave}(\underline{r}) = \frac{\sum_{i=1}^{3}\sigma_i(\underline{r})}{3}$ is the average of the eigenvalues;
  - Ω is the space region that defines the lens

- Far-Field Matching Error

$$\xi = \frac{\sum_{u=1}^{U}\sum_{v=1,\ (u,v)\notin\Omega}^{V}|E_{est}(\theta_u,\varphi_v)-E_{ref}(\theta_u,\varphi_v)|^2}{\sum_{u=1}^{U}\sum_{v=1,\ (u,v)\notin\Omega}^{V}|E_{ref}(\theta_u,\varphi_v)|^2} \tag{33}$$

- Near-Field Matching Error

$$\chi = \frac{\sum_{u=1}^{U}\sum_{v=1,\ (u,v)\notin\Omega}^{V}|E_{est}(x_u,y_v)-E_{ref}(x_u,y_v)|^2}{\sum_{u=1}^{U}\sum_{v=1,\ (u,v)\notin\Omega}^{V}|E_{ref}(x_u,y_v)|^2} \tag{34}$$

2 Numerical Results

2.1 Parameters

- Array:
  - Number of elements: $N = 6$
  - Radius of circular array: $r_{array} = 1.45\ [\lambda]$
  - Elements spacing: $d \simeq 0.52\ [\lambda]$
- Schwarz-Christoffel Transformation:
  - Virtual Region
    - Virtual ground plane radius: $r_{virt-gnd} = 1.2\ [\lambda]$
    - Distance from the ground plane: $\delta = r_{array} - r_{virt-gnd} = \frac{\lambda}{4}$
    - Virtual permittivity: $\varepsilon = 1$
    - Virtual permeability: $\mu = 1$
  - Physical Region
    - External radius: $L_{ext} = 2.5\ [\lambda]$
    - External Lens boundary : $\partial\Omega_{ext} = \left\{(x, y) \in \mathbb{R} \mid \sqrt{x^2 + y^2} = L_{ext}\right\}\ [\lambda]$
    - Internal Lens boundary: $\partial\Omega_{int} = \{(1.4; 0),\ (0; 0.3);\ (-1.4; 0),\ (0, -0.3)\}\ [\lambda]$
    - Number of points defining the external boundary: $n_{ext} = 24$
    - Number of points defining the internal boundary: $n_{int} = 4$
- SCTO parameters
  - Error tolerance: 10^{-10}
  - Number of Gauss-Jacobi points (nodes): 6
  - Discretization in virtual grid (outer boundary): $\Delta = 0.2\ [\lambda]$
- Simulation Tool
  - Working frequency: $f_w = 300\ [MHz]$
  - Simulation region: $\begin{cases} x \in [-20,\ 20]\ [\lambda] \\ y \in [-20,\ 20]\ [\lambda] \end{cases}$
  - Near-Field computation: $\begin{cases} x \in [-20,\ 20]\ [\lambda] \\ y \in [-20,\ 20]\ [\lambda] \end{cases}$
  - Far-Field computation: $\begin{cases} \theta = \frac{\pi}{2}\ [rad] \\ \varphi \in [0,\ \pi]\ [rad] \end{cases}$

- Mesh settings
  - Size: $size_{mesh} \in [5 \times 10^{-4}, 0.2]$
  - Maximum growth rate: 1.3
  - Curvature factor: 0.3
  - Narrow region resolution: 1
- Simulation region layer thickness: 1

2.2 Results

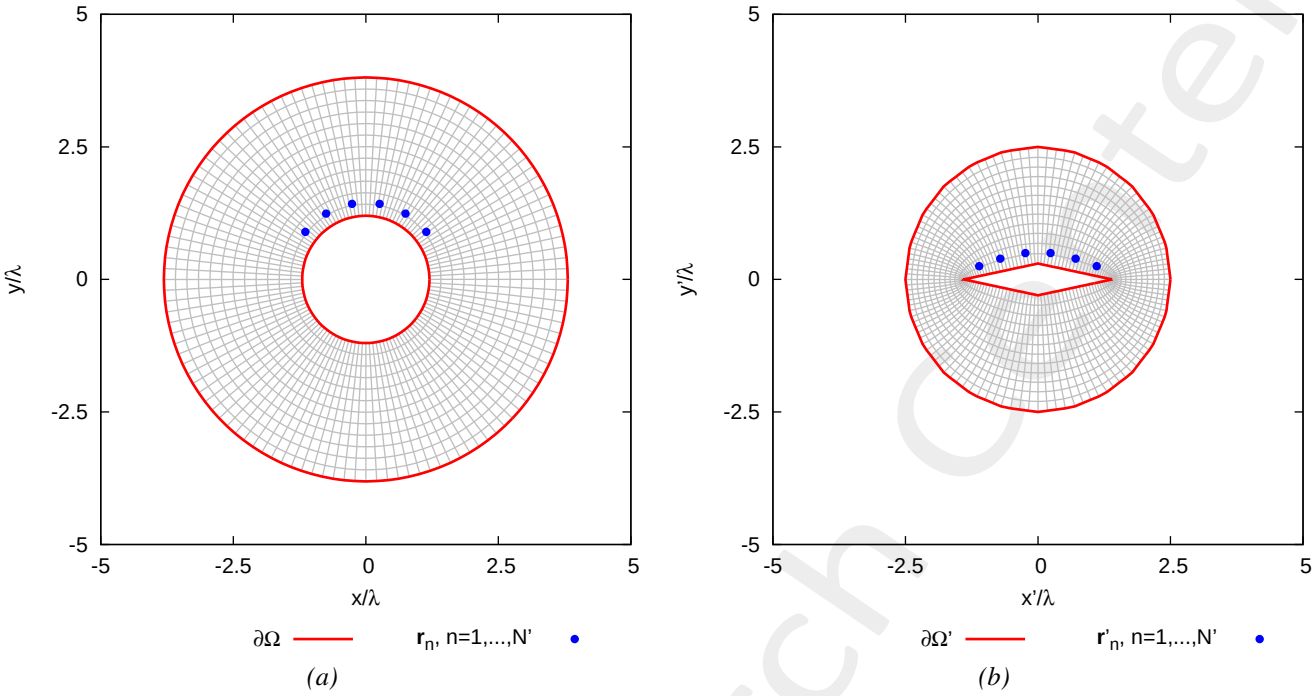

Figure 4: *(a)* Virtual and *(b)* Physical geometries

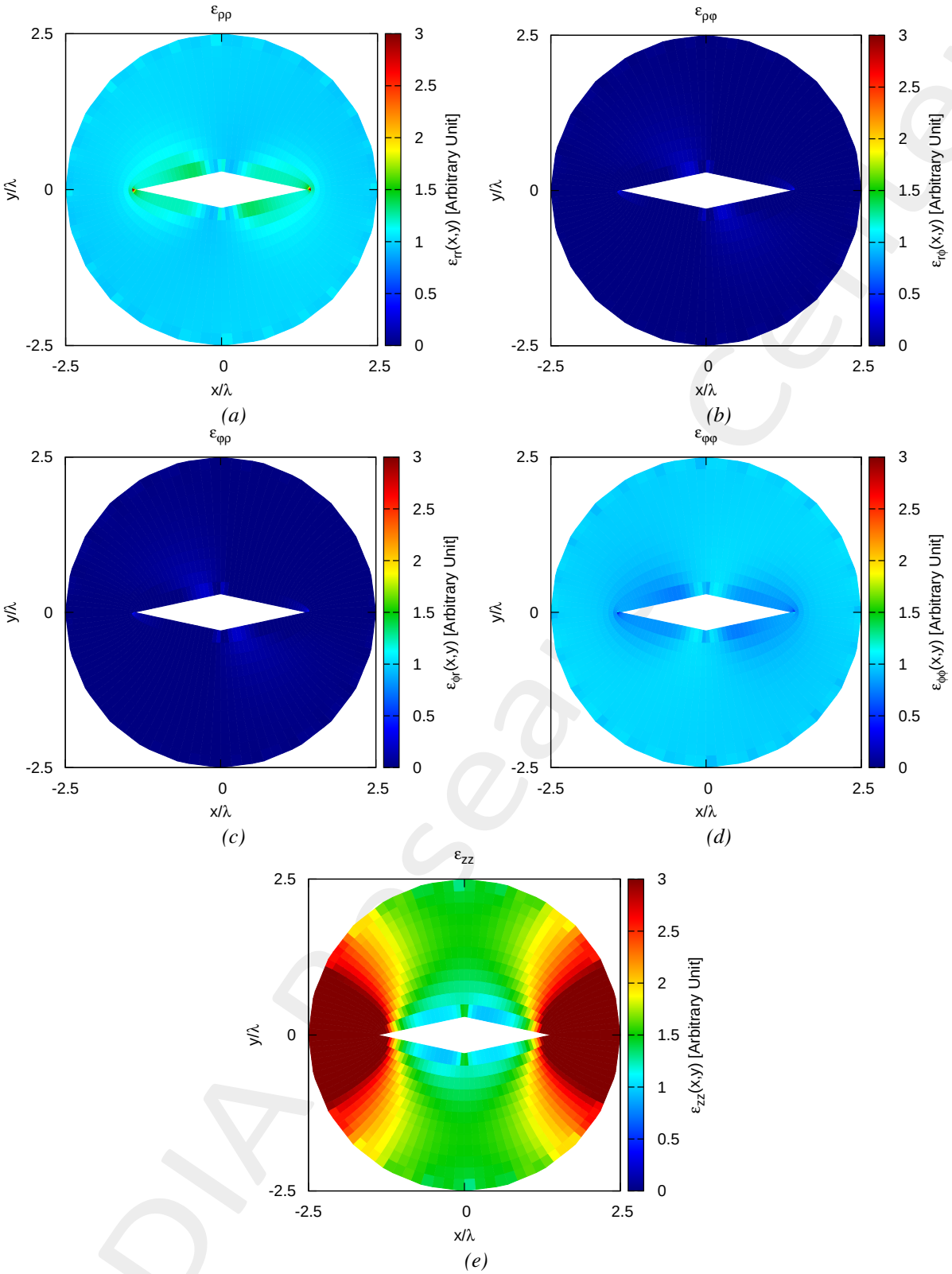

Figure 5: Tensor permittivity values for *(a)* $\varepsilon_{\rho\rho}$, *(b)* $\varepsilon_{\rho\varphi}$, *(c)* $\varepsilon_{\varphi\rho}$, *(d)* $\varepsilon_{\varphi\varphi}$, *(e)* ε_{zz}

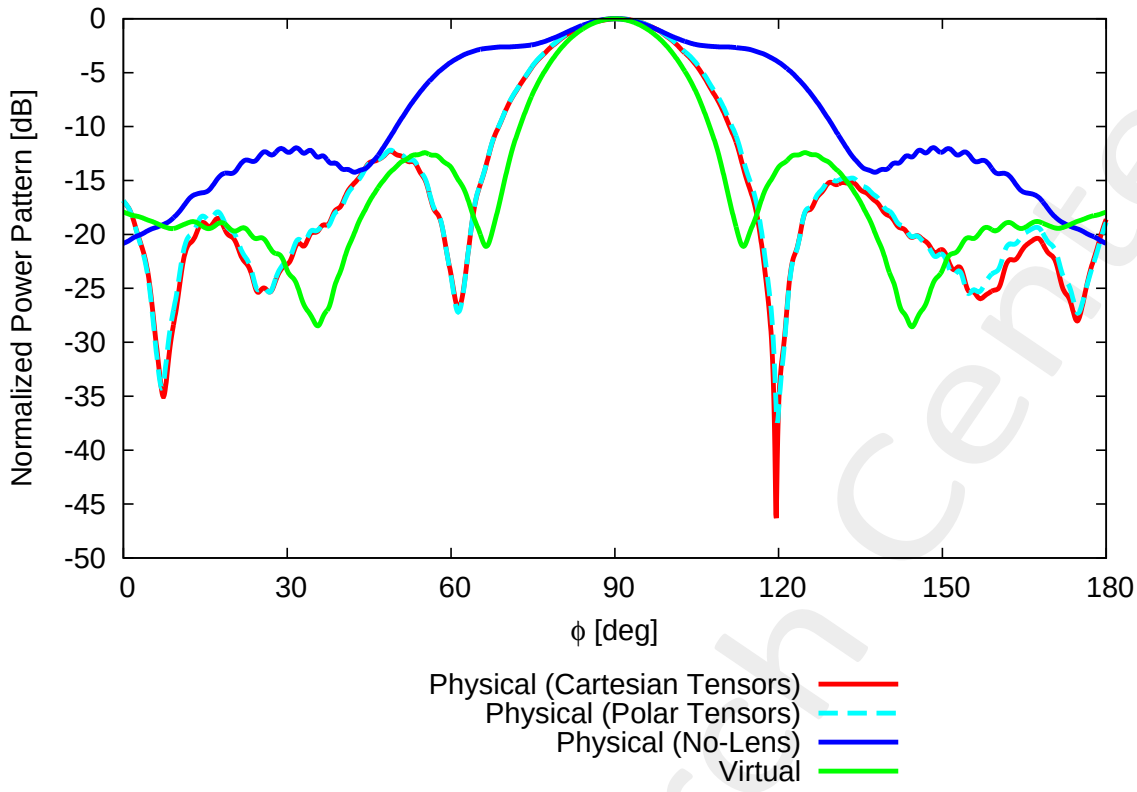

(a)

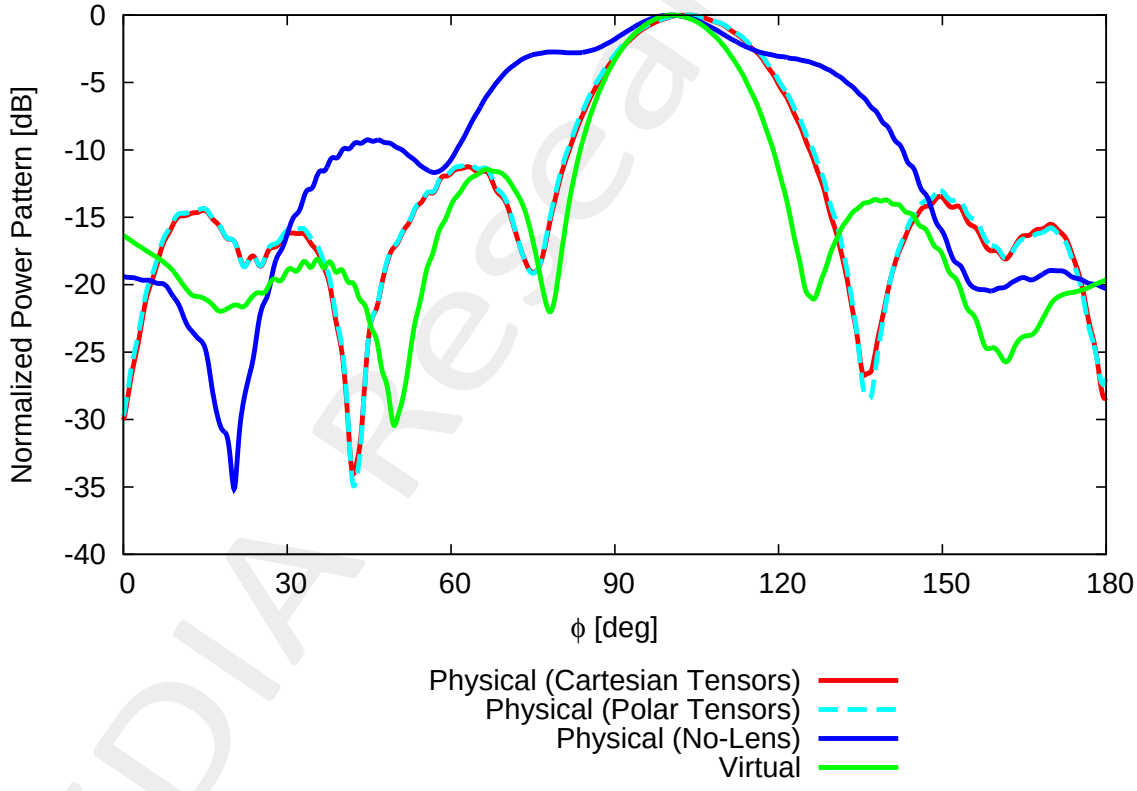

(b)

Figure 6: Far-Field Pattern for $\theta = 90$ [deg] and $\varphi \in [0, 180]$ [deg] for *(a)* broadside and *(b)* steering at $\varphi = 100$ [deg]

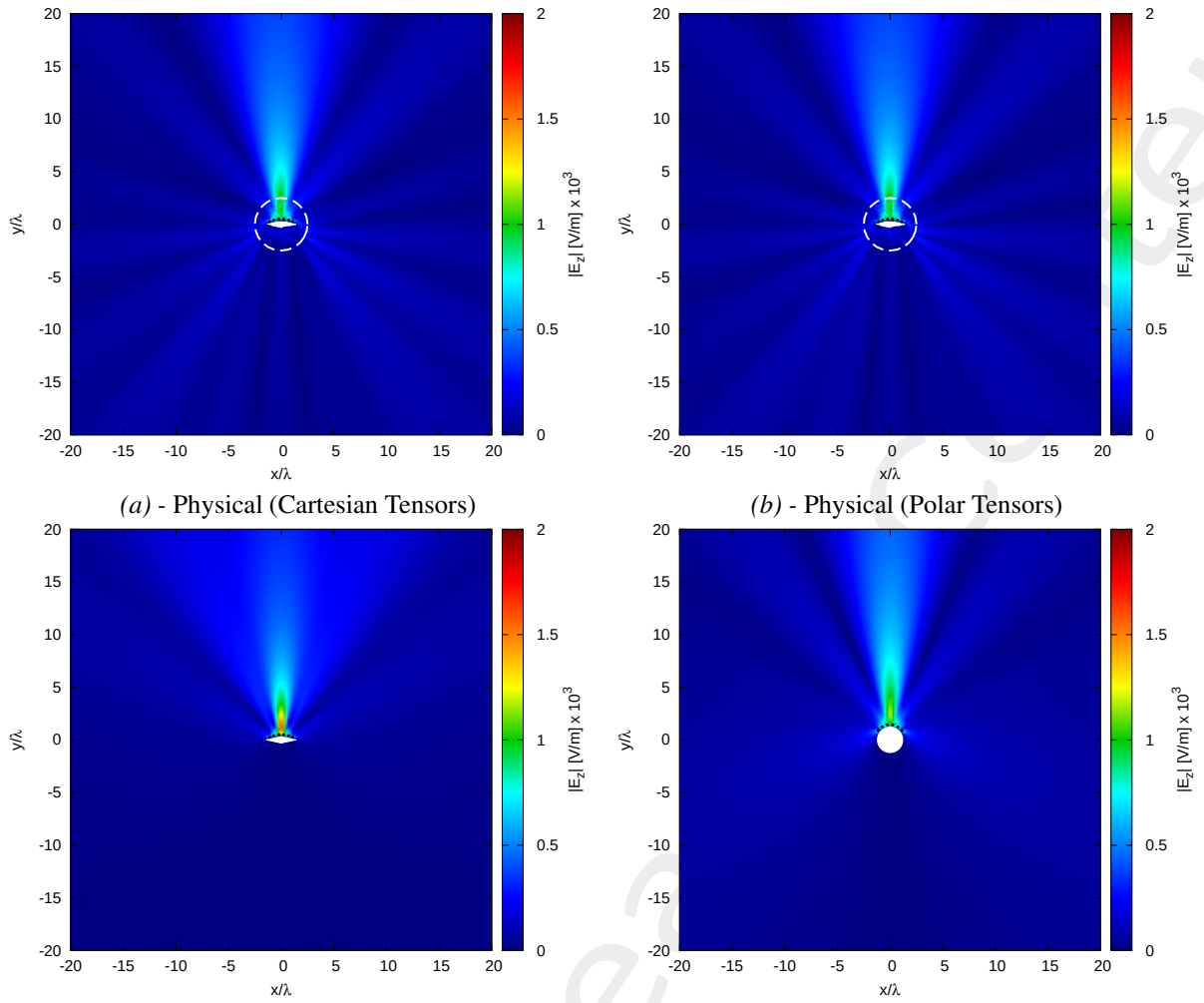

(a) - Physical (Cartesian Tensors)

(b) - Physical (Polar Tensors)

(c) - Physical (No Lens)

(d) Virtual

Figure 7: Near-Field pattern for *(a),(b),(c)* physical and *(d)* geometries

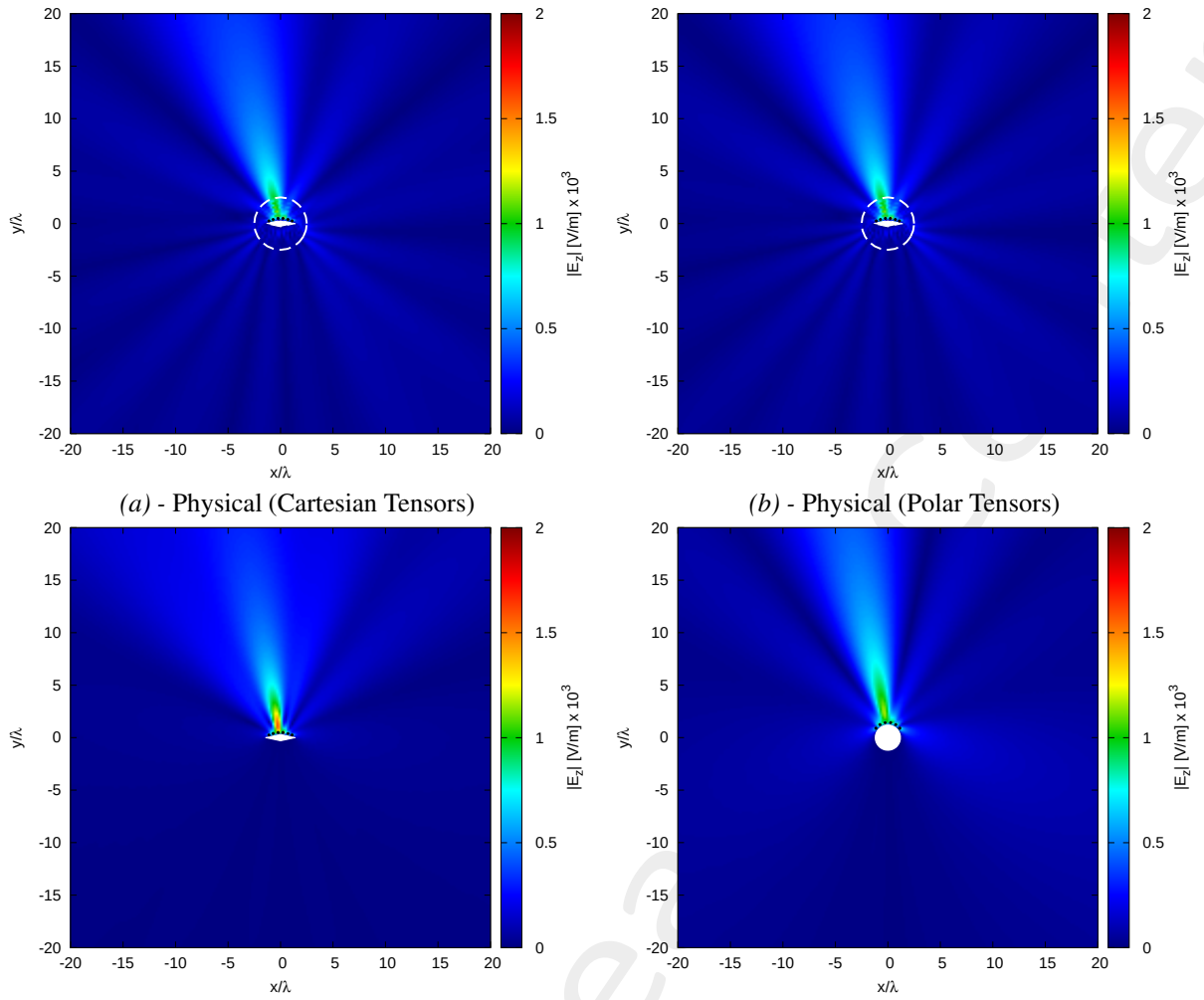

(a) - Physical (Cartesian Tensors)

(b) - Physical (Polar Tensors)

(c) - Physical (No Lens)

(d) Virtual

Figure 8: [Angle of Steering: $\alpha = 100$ [deg]] - Near-Field pattern for *(a),(b),(c)* physical and *(d)* geometries

3 Conclusions

An innovative transformation electromagnetics methodology leveraging on the Schwarz-Christoffel theory has been proposed to design conformal phased arrays. The preliminary numerical results have shown the effectiveness and the potential of the method.

References

[1] M. Salucci, F. Boulos, A. Polo, and G. Oliveri, “Conformal transformation electromagnetics based on Schwarz-Christoffel mapping for the synthesis of doubly-connected metalenses,” *IEEE Trans. Antennas Propag.*, vol. 68, no. 3, pp. 1836-1850, Mar. 2020.

[2] M. Salucci, L. Tenuti, G. Gottardi, A. Hannan, and A. Massa, "System-by-design method for efficient linear array miniaturisation through low-complexity isotropic lenses" *Electronic Letters*, vol. 55, no. 8, pp. 433-434, May 2019.

[3] M. Salucci, G. Oliveri, N. Anselmi, and A. Massa, "Material-by-design synthesis of conformal miniaturized linear phased arrays," *IEEE Access*, vol. 6, pp. 26367-26382, 2018.

[4] M. Salucci, G. Oliveri, N. Anselmi, G. Gottardi, and A. Massa, "Performance enhancement of linear active electronically-scanned arrays by means of MbD-synthesized metalenses," *Journal of Electromagnetic Waves and Applications*, vol. 32, no. 8, pp. 927-955, 2018.

[5] G. Oliveri, M. Salucci, N. Anselmi and A. Massa, "Multiscale System-by-Design synthesis of printed WAIMs for waveguide array enhancement," *IEEE J. Multiscale Multiphysics Computat. Techn.*, vol. 2, pp. 84-96, 2017.

[6] G. Oliveri, F. Viani, N. Anselmi, and A. Massa, "Synthesis of multi-layer WAIM coatings for planar phased arrays within the system-by-design framework," *IEEE Trans. Antennas Propag.*, vol. 63, no. 6, pp. 2482-2496, June 2015.

[7] A. Massa and G. Oliveri, "Metamaterial-by-Design: Theory, methods, and applications to communications and sensing - Editorial," *EPJ Applied Metamaterials*, vol. 3, no. E1, pp. 1-3, 2016.

[8] G. Oliveri, E. T. Bekele, M. Salucci, and A. Massa, "Transformation electromagnetics miniaturization of sectoral and conical horn antennas," *IEEE Trans. Antennas Propag.*, vol. 64, no. 4, pp. 1508-1513, April 2016.

[9] G. Oliveri, E. T. Bekele, M. Salucci, and A. Massa, "Array miniaturization through QCTO-SI metamaterial radomes" *IEEE Trans. Antennas Propag.*, vol. 63, no. 8, pp. 3465-3476, Aug. 2015.

[10] L. Tenuti, M. Salucci, G. Oliveri, P. Rocca, and A. Massa, “Surrogate- assisted optimization of metamaterial devices for advanced antenna Systems,” Proc. 2015 IEEE Symposium Series on Computational Intelligence (IEEE SSCI 2015), Cape Town, South Africa, pp. 1154-1156, Dec. 8-10, 2015.

[11] G. Oliveri, L. Tenuti, M. Salucci, and A. Massa, “Innovative antenna architectures exploiting metamaterials for new generation radars,” 10th European Conference on Antennas and Propagation (EUCAP 2016), Davos, Switzerland, pp. 1-3, April 11-15, 2016.

[12] M. Salucci, G. Oliveri, H. Ahmadi, and A. Massa, "Conformal transformation of linear arrays through QCTO-based design tools," Proc. 2016 IEEE AP-S International Symposium and USNC-URSI Radio Science Meeting, Fajardo, Puerto Rico, pp. 1083- 1084, July 26 - July 1, 2016.

[13] M. Salucci, L. Tenuti, E. Bekele, and G. Oliveri, "Enhancement of linear arrays through MbD metamaterial coatings," Proc. 2016 IEEE AP-S International Symposium and USNC-URSI Radio Science Meeting, Fajardo, Puerto Rico, pp. 1089- 1090, July 26 - July 1, 2016.

[14] P. Rocca, N. Anselmi, A. Polo, and A. Massa, "An irregular two-sizes square tiling method for the design of isophoric phased arrays," *IEEE Trans. Antennas Propag.*, vol. 68, no. 6, pp. 4437-4449, Jun. 2020.

[15] P. Rocca, N. Anselmi, A. Polo, and A. Massa, "Modular design of hexagonal phased arrays through diamond tiles," *IEEE Trans. Antennas Propag.*, vol.68, no. 5, pp. 3598-3612, May 2020.

[16] N. Anselmi, L. Poli, P. Rocca, and A. Massa, "Design of simplified array layouts for preliminary experimental testing and validation of large AESAs," *IEEE Trans. Antennas Propag.*, vol. 66, no. 12, pp. 6906-6920, Dec. 2018.

[17] N. Anselmi, P. Rocca, M. Salucci, and A. Massa, "Contiguous phase-clustering in multibeam-on-receive scanning arrays" *IEEE Trans. Antennas Propag.*, vol. 66, no. 11, pp. 5879-5891, Nov. 2018.

[18] N. Anselmi, P. Rocca, M. Salucci, and A. Massa, "Irregular phased array tiling by means of analytic schemata-driven optimization," *IEEE Trans. Antennas Propag.*, vol. 65, no. 9, pp. 4495-4510, Sept. 2017.

[19] N. Anselmi, P. Rocca, M. Salucci, and A. Massa, "Optimization of excitation tolerances for robust beamforming in linear arrays" *IET Microwaves, Antennas & Propagation*, vol. 10, no. 2, pp. 208-214, 2016.